HIPPOCAMPUS 18:1270–1282 (2008)

Influence of Boundary Removal on the Spatial Representations of the Medial Entorhinal Cortex

Francesco Savelli, D. Yoganarasimha, and James J. Knierim*

ABSTRACT: The medial entorhinal cortex (MEC) is thought to create and update a dynamical representation of the animal's spatial location. Most suggestive of this process are grid cells, whose firing locations occur periodically in space. Prior studies in small environments were ambiguous as to whether all spatially modulated cells in MEC were variants of grid cells or whether a subset resembled classic place cells of the hippocampus. Recordings from the dorsal and ventral MEC were performed as four rats foraged in a small square box centered inside a larger one. After 6 min, without removing the rat from the enclosure, the walls of the small box were quickly removed, leaving the rat free to continue foraging in the whole area enclosed by the larger box. The rate-responses of most recorded cells (70 out of 93 cells, including 15 of 16 putative interneurons) were considered spatially modulated based on information-theoretic analysis. A number of cells that resembled classic hippocampal place cells in the small box were revealed to be grid cells in the larger box. In contrast, other cells that fired along the boundaries or corners of the small box did not show grid-cell firing in the large box, but instead fired along the corresponding locations of the large box. Remapping of the spatial response in the area corresponding to the small box after the removal of its walls was prominent in most spatially modulated cells. These results show that manipulation of local boundaries can exert a powerful influence on the spatial firing patterns of MEC cells even when the manipulations leave global cues unchanged and allow uninterrupted, self-motion-based localization. Further, they suggest the presence of landmark-related information in MEC, which might prevent cumulative drift of the spatial representation or might reset it to a previously learned configuration in a familiar environment.

KEY WORDS: grid cell; place cell; single unit; hippocampus; multiple electrodes

INTRODUCTION

The entorhinal cortex is the major conduit of information from the neocortex into the hippocampus. The medial entorhinal cortex (MEC) conveys spatial information into the hippocampus (Barnes et al., 1990; Quirk et al., 1992; Fyhn et al., 2004), whereas the lateral entorhinal cortex (LEC) appears to lack spatial firing properties (Hargreaves et al., 2005). Moreover, the firing fields of neurons in the dorsocaudal region of MEC show a highly regular, periodic firing pattern. These cells have been termed "grid cells" because of the triangular (or hexagonal), grid-like pattern of their spatial firing (Hafting et al., 2005; Sargolini et al., 2006; Moser and Moser, 2008). It is believed that the grid cell phenomenon is a reflection of a self-motion based, path-integration computation (Hafting et al., 2005; O'Keefe and Burgess, 2005; Fuhs and Touretzky, 2006; McNaughton et al., 2006; Burgess et al., 2007; Hasselmo et al., 2007; Blair et al., 2008; Burgess, 2008; Hasselmo, 2008; Giocomo and Hasselmo, 2008). That is, the firing of grid cells is thought to be controlled predominantly by internal mechanisms, as opposed to external landmarks, with the animal's self-motion as the metric of distances and angular heading in an environment (but see Franzius et al., 2007; Kropff and Treves, 2008 for models of grid activity emerging from slow adaptation to pre-existing spatial stimuli). External landmarks play an important supporting role in this path-integration computation by binding the internally generated, grid-cell representation to the external world (McNaughton et al., 2006; Barry et al., 2007; Fyhn et al., 2007; see also Hasselmo, 2008).

Early investigations of the firing of MEC neurons did not reveal the grid-like firing of MEC neurons (Barnes et al., 1990; Quirk et al., 1992). There are a number of potential explanations for this early failure to observe the phenomenon. First, the scale at which grid cells tessellate the environment varies with anatomical location along the dorsal–ventral axis of the MEC, with the most fine-scale grid cells located at the most dorsocaudal region of the MEC, the region that projects to the most dorsal (septal) part of the hippocampus, where most place cell recordings are performed (Dolorfo and Amaral, 1998; Fyhn et al., 2004; Brun et al., 2008). In most standard-sized recording chambers or mazes, the grid cell pattern would be apparent only when recordings came from this most dorsocaudal location, and the prior studies recorded from regions that were rostral and ventral to this zone. Second, the grid pattern may be most apparent only when the animal is moving in an open field, such that all locations on a two-dimensional surface are sampled; thus, a recording on a radial eight-arm maze, for example, would not necessarily reveal the grid-like firing pattern (Barnes et al., 1990; see also Lipton et al., 2007).

Department of Neurobiology and Anatomy, University of Texas Medical School at Houston, Houston, Texas
Grant sponsor: National Institute of Neurological Disorders and Stroke; Grant number: R01 NS39456. Grant sponsor: International Human Frontier Science Program Organization; Grant number: LT00683/2006-C.
*Correspondence to: James J. Knierim, Department of Neurobiology and Anatomy, University of Texas Medical School at Houston, P.O. Box 20708, Houston, TX 77225, USA. E-mail: james.j.knierim@uth.tmc.edu
Accepted for publication 2 September 2008
DOI 10.1002/hipo.20511
Published online 19 November 2008 in Wiley InterScience (www.interscience.wiley.com).

Hargreaves et al. (2005) recorded from MEC cells located in regions that projected to the dorsal hippocampus, but not as extremely dorsocaudal as the region where the highest-resolution grid cells are found. Subsequently, because the size of the recording environment (67 cm × 67 cm, 51 cm high) was relatively small, the spatial firing of the MEC neurons in that study did not show obvious grid-cell patterns. Rather, the firing fields of many spatially selective cells of Hargreaves et al. (2005) looked very similar to hippocampal place fields, with primarily single firing fields or with 2–3 fields spaced apart in the recording box. There are two possible interpretations of this result. One interpretation is that these cells were grid cells that fired at an intermediate grid resolution, such that only 1–3 vertices of the grid were contained in the square chamber. Another interpretation is that classic place cells or other spatially modulated cell types may be intermixed with grid cells, at least in this region of the MEC.

To address these two possible interpretations, we recorded cells from regions along the dorsal–ventral axis of MEC in both small- and large-box environments. Rats initially foraged for food reward in a small box with removable walls. Under these conditions, discrete place fields similar to those of Hargreaves et al. (2005; Quirk et al., 1992) were recorded, as well as multiple-peaked firing in the more dorsocaudal regions. After 6–7 min of foraging in the small box, the walls were removed in the presence of the rat, revealing a much larger box. If the single-peaked firing fields in the small box were really grid cells, then the grid-pattern should become evident in the larger box as more grid vertices appear when the rat explores the larger box. Alternatively, if the single-peaked fields were really classic place fields (such as are found in the hippocampus proper), then the cells should show similar firing in the larger box. The results showed that both types of responses were observed: some cells revealed themselves to be grid cells in the larger box, whereas other cells showed single-peaked firing in both boxes. The latter group was dominated by cells that fired along a wall or corners in both boxes, properties that might play a role in binding the path-integration-based grid-cell representation to the boundaries of a given environment (Barry et al., 2007), or in resetting the path integration process to prevent errors in self-motion information from accumulating over time (Burgess et al., 2007). The strong influence of the boundaries was also reflected in changes to the spatial firing of the cells in the small box and the large box, as removal of the walls caused location changes and/or rate changes in the large majority of cells.

MATERIALS AND METHODS

Subjects and Surgery

Four male Long-Evans rats, aged 5–6 months and weighing 540–760 g at time of surgery, were housed individually on a 12:12 h reversed light–dark cycle, and recordings were performed during the dark portion of the light–dark cycle. During behavioral training and recordings, rats were maintained at 80–90% of their free-feeding weights. Animal care, surgical procedures, and euthanasia were performed in accordance with the National Institutes of Health (NIH) and the University of Texas Health Science Center at Houston Institutional Animal Care and Use Committee (IACUC) guidelines.

Under surgical anesthesia, a custom-built recording drive (hyperdrive), allowing the independent manipulation of 20 recording probes (18 tetrodes with two reference electrodes for differential recording), was implanted over the right hemisphere. The recording probes, arranged inside a 1.8-mm inner diameter stainless steel cannula, were implanted such that they made vertical penetrations through the brain. The most posterior tetrode in the hyperdrive was positioned 4.8–5.0 mm lateral to the midline and 600–800 μm anterior to the transverse sinus. The tetrode array afforded access to neurons along the dorsocaudal to ventral axis of the MEC. Immediately after the surgery, the rats were given ketoprofen (5 mg/kg) subcutaneously for analgesia, and they received daily doses of tetracycline (30 mg/day) and baytril (0.15 cm^3/day) mixed with their food until the completion of the experimental procedures.

Training

After 5–6 days of surgical recovery, the rats were trained to forage in a large box for food reward (chocolate sprinkles). The large box (135L × 135W × 30H cm) was placed on the floor on brown wrapping paper next to the recording system and computer in a dimly lit room (Fig. 1). The room had white colored walls and ceiling, with shelves on one wall and doors and other salient cues on the other three walls.

For training in the large box, the rat was placed on a pedestal next to the box, connected with recording cables, transferred into the box, and allowed to forage freely, searching for food reward. The chocolate sprinkles were thrown into different locations of the box for complete coverage of the box arena. Each rat had 30 min of training daily, over a period of 10–14 days, before the start of recording sessions. The tetrodes were advanced to the MEC area during this period and were also lowered after each day of recording to sample different cells on subsequent days.

Experimental Protocol

After training, a foraging session was recorded daily for several days. The recording stability was assessed with baseline data collected from the rat during sleep or awake immobility for 20–30 min before and after the foraging sessions. After the first baseline session, the rat was placed in a small box (58L × 58W × 30H cm) located in the center of the large box used for training (as described earlier), on the floor next to the recording system and computer. The perimeter of the small box was composed of two L-shaped halves that allowed its removal without removing the rat or otherwise interrupting the session. The rat was allowed to forage for 6 min in the small box, and then the walls of the small box were quickly removed in the

FIGURE 1. Recording apparatus. The foraging session was initiated in the small box centered inside the large box. The small box was composed of two L-shaped walls, which allowed its rapid removal after the rat explored the small box for ~6 min (PRE epoch). The rat was then free to continue foraging in the large box for the remainder of the session (POST epoch, ~34 min).

presence of the rat. The removal operation took ~10–20 s. The rat was then allowed to forage in the large box for the next 34 min. The amount of foraging time in each box was approximately proportional to the surface area of each box. Upon completion of foraging, the rat was placed onto the pedestal and a second baseline session was recorded while the rat slept or sat quietly on a pedestal.

Recording Electronics

After postsurgical recovery, the tetrodes were slowly advanced to the entorhinal cortex over the course of several days, while the rat sat quietly on a pedestal next to the recording electronics. Recording locations in MEC were estimated by monitoring changes in EEG patterns and changes in the neural activity levels as the tetrodes advanced through cortex and white matter. The appearance of theta rhythm in the EEG and/or grid-cell firing properties in test recordings in the large box on any of the tetrodes signaled that those tetrodes were likely to be in MEC. One or more tetrodes (typically one of the reference electrodes) were advanced to find the depth of the Layer I–Layer II border, which was identified by a reversal in the phase of the theta rhythm (Alonso and Garcia-Austt, 1987). Other tetrodes were adjusted relative to these "guide" tetrodes based on their relative locations in the bundle, their depths from the brain surface, and comparisons with brain atlas images (Paxinos and Watson, 1998). The experiments commenced when a majority of tetrodes were estimated to be in the superficial layers of MEC. Final determination of recording sites was performed postmortem using standard histological analyses (see later).

Recordings were performed with the Cheetah Data Acquisition System (Neuralynx, Bozeman, MT). Neural signals were amplified between 2,000 and 10,000 times, filtered between 600 Hz and 6 kHz, digitized at 32 kHz, and stored on a PC computer. The headstage, which was connected to an electrode interface board on the hyperdrive, contained a circular array of LEDs (5 red LEDs in front and 5 blue LEDS in back) and a boom arm that extended two green LEDs 15 cm behind the headstage. The output of the video camera mounted on the ceiling was captured by a video frame grabber (DT3120, Data Translation, Marlboro, MA) at 30 Hz. The position of the rat at each frame was defined as the center of mass (COM) of all blue and red pixels, and the head direction was defined as the angle between the COM of the blue and red pixels and the COM of the green pixels.

Spike Sorting and Analysis

Neural data acquired during baseline and foraging sessions were subjected to offline analysis. Single units were isolated primarily based on the relative amplitudes of signals recorded simultaneously at four slightly different locations on the tetrode. Additional waveform characteristics, such as spike width, were also considered. Scatter plots of the waveform parameters from one of the channels versus another were created and, with the use of a custom interactive program running on a PC workstation, boundaries were drawn around clusters of points formed by the individual units on the scatter plots. Based on the size of the waveforms relative to background and on the closeness and degree of potential overlap between neighboring

clusters, the isolation quality of a cell was rated on a subjective scale of 1 (very well-isolated) to 4 (marginally isolated), independent of the spatial firing characteristics of the cell. All cells rated 4 (marginally isolated) were excluded from the analysis.

Spike width was employed to help discriminate between putative interneurons and principal cells, along with the mean firing rate (mfr). The spike width was measured as the time interval between the peak of the spike event and the first valley following it.

Spatial Information Analysis

To determine which cells had a spatial response that was consistent over time, we calculated the mutual information (Shannon and Weaver, 1949; Cover and Thomas, 2006) between the position x occupied by the rat and the cell's firing rate response r. This spatial information (SI) score can be seen as a measure of the statistical dependence of x and r, or as a measure of how better the value of one variable can be predicted if the other is known. For this analysis, the area enclosed in the large box was segmented into 10 cm $\times$ 10 cm bins. For the large-box session following the small-box wall removal, every visit of the rat to a bin was divided into 100 ms time intervals, and the spikes fired by the cell in each interval were counted. Visits to a single bin that lasted more than 10 s were discarded to prevent the inclusion of spikes fired during long periods of inactivity. The spike count was used to determine whether the firing rate in the time interval was above (high firing: H) or below (low firing: L) the mfr averaged over the entire session following the removal of the small box. The response variable r is therefore binary $r = \{H, L\}$. Representing the rat's position as the variable x that ranges over the spatial bins x_i, the marginal probabilities $P(x_i)$, $P(H)$, and $P(L)$, and the conditional probabilities $P(H|x_i)$ and $P(L|x_i)$ were estimated based on the frequency with which the values taken by x and r occurred across all the time intervals. The mutual information SI between x and r is then given by:

$$\mathrm{SI} = \sum_i P(x_i)\left\{ P(H|x_i)\log_2\left[\frac{P(H|x_i)}{P(H)}\right] + P(L|x_i)\log_2\left[\frac{P(L|x_i)}{P(L)}\right]\right\}$$

Spatial bins that received fewer than five distinct visits or a total visit time of less than 5 s were considered under-sampled for estimating the related probabilities and were excluded from the calculation of SI (note that each bin would be occupied for more than 11 s if the duration of the postremoval epoch were divided equally among all of them).

The only substantial difference between similar previous analyses (Olypher et al., 2003; Ego-Stengel and Wilson, 2007; Wilent and Nitz, 2007) and our calculation lies in our choice to characterize the cell's rate response with a binary code—above or below the cell's mfr—as opposed to discretizing the response from 0 Hz to its maximum value by a variable number of fixed-size rate bins. This choice was dictated by the poorer spatial sampling produced by open-field rat exploration when compared with the linear tracks used in the previous studies (Ego-Stengel and Wilson, 2007; Wilent and Nitz, 2007). Limited sampling can cause mutual information to be overestimated (Miller, 1955; Treves and Panzeri, 1995; Panzeri et al., 2007). For example, even when the mutual information between two variables is 0 (because they are statistically independent), any less-than-ideal estimation of the statistical distributions involved in its computation will produce a spurious amount of mutual information, because information is positive by definition and so must be any deviation from the correct 0 value. The size of the probability table representing the conditional distribution in our problem is given by the product of the number of spatial and firing-rate bins. By reducing the binning resolution of either variable, we can reduce the spurious information because more data become available for each entry of the table. To estimate the spurious information, we used 100 random shufflings of the spike counts relative to their associated positions in space—hence breaking any potential statistical dependence between space and firing (Optican et al., 1991). Using the cell's mfr to separate the two response regions permitted a binary code scaled on the individual cell's level of activity that did not commit the significance of the analysis to a baseline firing level assumed a priori for all cells.

Rate Map Analysis

Firing rate maps were created by segmenting the box environment into 3.2 cm^2 bins and, for each bin, dividing the number of spikes fired by the overall amount of time spent by the rat in that bin. Bins that were not visited were excluded from further analysis. Rate maps were smoothed with the adaptive binning algorithm of Skaggs et al. (1996) for visualization purposes, or with a 5 $\times$ 5 bin Gaussian kernel of variance 3.2 cm when used for further analysis.

To expose the periodic structure characteristic of the spatial response of a potential grid cell, we computed the spatial autocorrelogram of its rate map (Hafting et al., 2005). Each pixel of the autocorrelogram was the Pearson correlation coefficient between the bins of the rate map and the corresponding bins of the rate map shifted along each axis by a discrete number of bins. These offsets τ_x and τ_y identified the position of the pixel on the autocorrelogram. Mathematically,

$$r(\tau_x,\tau_y) = \frac{n\sum\lambda(x,y)\lambda(x-\tau_x,y-\tau_y) - \sum\lambda(x,y)\lambda(x-\tau_x,y-\tau_y)}{\sqrt{n\sum\lambda(x,y)^2 - \left(\sum\lambda(x,y)\right)^2}\sqrt{n\sum\lambda(x-\tau_x,y-\tau_y)^2 - \left(\sum\lambda(x-\tau_x,y-\tau_y)\right)^2}}$$

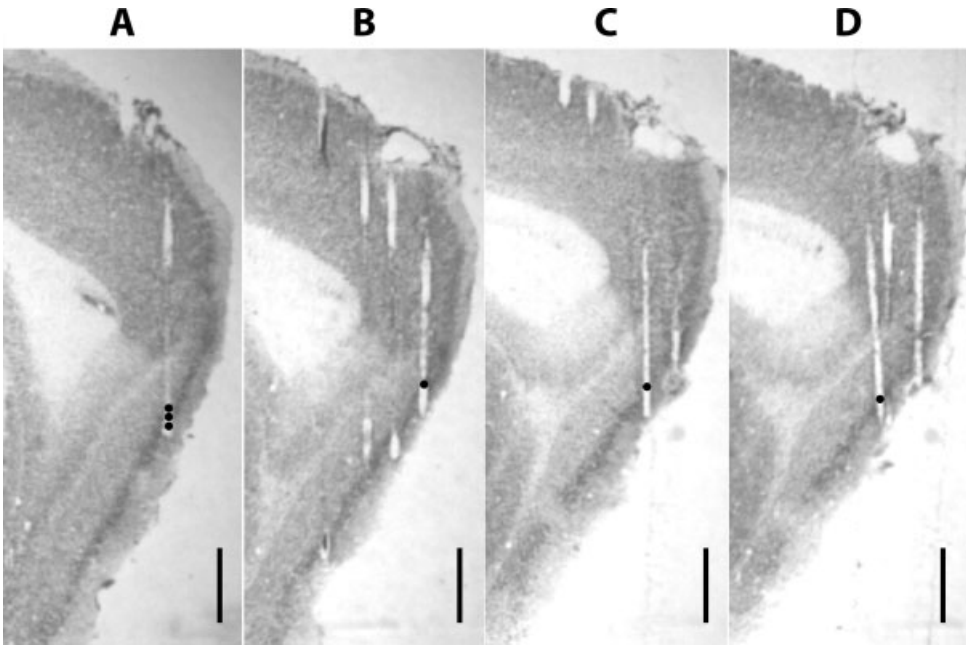

FIGURE 2. Representative tetrode tracks from MEC recordings (rat 191). The dots indicate the recording sites where cells with boundary-related activity were recorded. (A) The three black-filled circles indicate the progressively ventral recording locations of tetrode 17 on Days 6, 7, and 8 (from the top), where Cells 15, 16, 18, 19, 25, and 26 (see Fig. 4) were recorded. (B) Position of tetrode 18 on Day 5, where Cell 17 was recorded. (C) Position of tetrode 3 on Day 3, where Cell 24 was recorded. (D) Position of tetrode 1 on Day 3, where Cell 23 was recorded. Scale bar = 1 mm.

where $r(\tau_x, \tau_y)$ is the correlation coefficient in the pixel (τ_x, τ_y) of the autocorrelogram, and $\lambda(x,y)$ is the firing rate in the bin (x,y) of the firing rate map. We quantified the "gridness" of the cell's response based on the periodicity of the peaks appearing in the autocorrelogram, according to methods devised by Sargolini et al. (2006). The peaks were defined as sets of at least 20 contiguous bins with correlation coefficient ≥ 0.1 and were ordered according to the distance of their COM from the center of the autocorrelogram. The annulus between an inner circle around the central peak and an outer circle passing around the six peaks closest to the center (excluding the central peak) was selected. This area was rotated in incremental steps, and the Pearson correlation coefficient was computed between the rotated and nonrotated area. The gridness score was given by the difference between the lowest correlation at 60° and 120° and the highest correlation at 30°, 90°, and 150°.

To measure the degree to which the spatial pattern of firing scaled from the small to the large box, we computed the Pearson correlation coefficient between the firing rate map resulting from the small box exploration and a scaled version of the rate map representing the subsequent large box exploration. The latter map was computed after scaling down the coordinates of the rat's tracked positions so that the two maps had an identical distribution of spatial bins that allowed for the computation of the correlation coefficient.

Histology

Upon completion of the experiments, marker lesions were made on a subset of the tetrode tips by passing 10 μA current for 10 s. One day later, the rats were perfused transcardially with 4% formalin, after which the brain was extracted and kept in 30% sucrose formalin solution until the brain sank in the solution. Sagittal sections of 40 μm thickness were cut on a microtome, mounted, and stained with 0.1% cresyl violet. Digital photomicrographs were taken for all serial sections, and the electrode tracks were then compared with the configuration of the tetrode bundles and marker lesions, to identify which track corresponded to which tetrode. After the electrode tracks were identified, a depth reconstruction of the tetrode track was carried out for each recording session, to identify the specific layers of the MEC region where the cells were recorded.

RESULTS

We recorded from superficial and deep layers of the MEC area in four rats, over a total of 36 days (rat 159: 11 days; rat 165: 7 days; rat 174: 10 days; rat 191: 8 days). Figure 2 shows representative tetrode tracks in the MEC for one rat. Based on spike-sorting quality (see Materials and Methods section) and behavioral sampling quality, 93 cells met our analysis inclusion criteria (87 superficial layer cells, 6 deep layer cells). Pure head direction cells were also excluded. For each rat, 15–16 tetrodes were localized to MEC (dorsal and ventral), but not every tetrode yielded high-quality units. The 93 accepted cells were recorded from a total of 30 tetrodes in MEC (rat 159: 20 cells from seven tetrodes; rat 165: 17 cells from six tetrodes; rat

174: 19 cells from seven tetrodes; rat 191: 37 cells from ten tetrodes). We did not attempt to track units across days, but since recording tetrodes were lowered daily to increasingly ventral positions, it is unlikely that the same cell was included on multiple days.

Extent of Spatial Response in MEC

To address whether the spatial response of MEC cells varied after removing the small box walls, we first needed to determine which cells had firing that correlated with space. A natural solution to this problem is to measure the spatial information—in the sense of Shannon's Information Theory (Shannon and Weaver, 1949; Cover and Thomas, 2006), conveyed by the spiking rate of the cell. The most common analysis of this type is an information score (Skaggs et al., 1993, 1996) that measures the rate of spatial information per spike fired by the cell. However, this measure is insensitive to the consistency of the spatial response over time, and it is optimized for cells that concentrate their activity in a limited region of the recording area, like place cells of the hippocampus proper. We therefore opted for the direct calculation of the mutual information between the location of the rat and the cell's firing rate (SI, see Materials and Methods section), similar to previous analyses that detected temporally consistent spatial modulation in excitatory as well as inhibitory cells of the hippocampus proper, regardless of the spatial extent and intensity of their firing (Ego-Stengel and Wilson, 2007; Wilent and Nitz, 2007).

Figure 3A shows the SI and mfr values of the 93 cells in the large box after removing the small box walls. Solid circles represent the 70 cells that had SI at least three times greater than the maximum SI value found after shuffling the position data relative to the spike data. Empty circles denote the cells that did not pass this test, and thus they were excluded from further analysis. This test was primarily concerned with retaining only those cells whose firing rate conveyed substantially more spatial information than expected from limited-sampling estimation errors. Although the test's threshold was individually calculated for each cell, nearly all solid circles in Figure 3A are above SI = ~0.025 bits, whereas nearly all empty circles are below this level. Therefore, the spurious information due to limited sampling was of similar magnitude (~0.008 bits) across all cells and sessions.

Figure 3A shows that 15 of 16 cells with mfr > 10 Hz passed the spatial modulation test. These cells formed a separate cluster from the rest of the cells when their mfr was plotted against their spike width (Fig. 3B). Cells with mfr > 10 Hz were therefore considered putative interneurons, and those with mfr < 10 Hz were considered putative principal excitatory cells (Fox and Ranck, 1981; Frank et al., 2001; Hargreaves et al., 2005). Thus, similar to interneurons of the hippocampus proper, putative MEC interneurons showed a significant degree of spatial tuning in their firing properties (McNaughton et al., 1983; Kubie et al., 1990; Frank et al., 2001; Marshall et al., 2002; Ego-Stengel and Wilson, 2007; Wilent and Nitz, 2007).

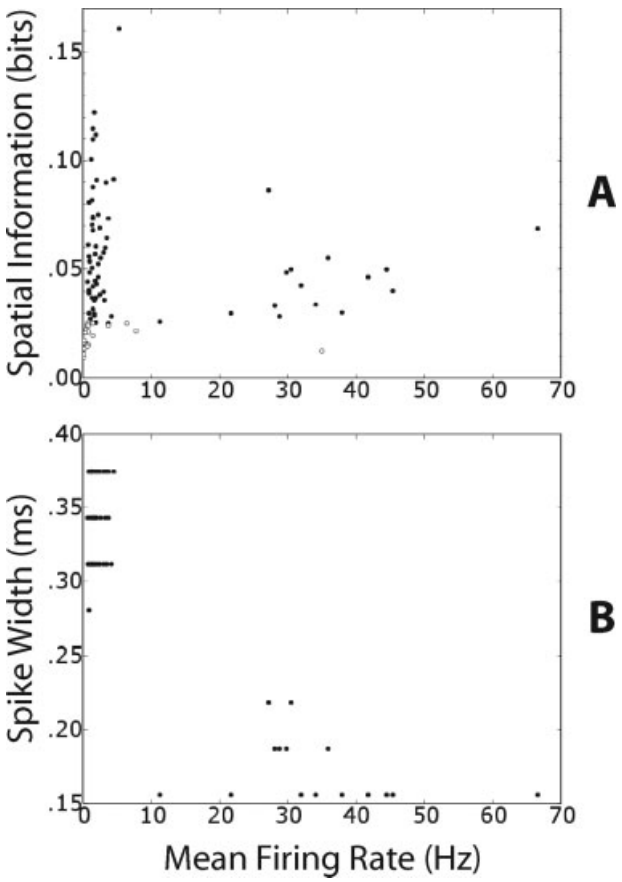

FIGURE 3. Spatial modulation of putative principal cells and interneurons. (A) Scatter plot of mean firing rate (mfr) and spatial information (SI) of all 93 cells. Both measures refers to the epoch of the session that occurred in the entire large box after the removal of the small-box walls. Filled circles denote cells (n = 70) that had a SI greater than three times the maximum SI computed with 100 random shufflings of the cell's spike train and the rat's location (see Materials and Methods section). Open circles denote the cells that did not pass this test and were excluded from the remapping analysis (n = 23). Note that the two populations are above and below ~0.025 bits, respectively, even though the spurious information was estimated individually for each cell. (B) Scatter plot of the mfr and spike width of the 70 cells that are represented by filled circles in A. Two distinct clusters represent putative principal cells (mfr < 10 Hz) and putative interneurons (mfr > 10 Hz).

Grid Cells and Boundary-Related Cells in MEC

The range of SI values in Figure 3A is representative of the varying degree of spatial tuning in putative principal cells, as evaluated qualitatively by visual inspection of their firing-rate maps. Figure 4 illustrates all the putative principal cells (mfr < 10 Hz) with SI > 0.05 bits (31 cells). Most of them displayed a degree of spatial selectivity that is comparable with typical place cells or grid cells. For each cell, the small figure at the upper left shows the firing rate map in the small box, and the large figure at right shows the firing rate map in the large box. The small figure at the lower left shows the portion of the large-box rate map that corresponds to the area of the small box.

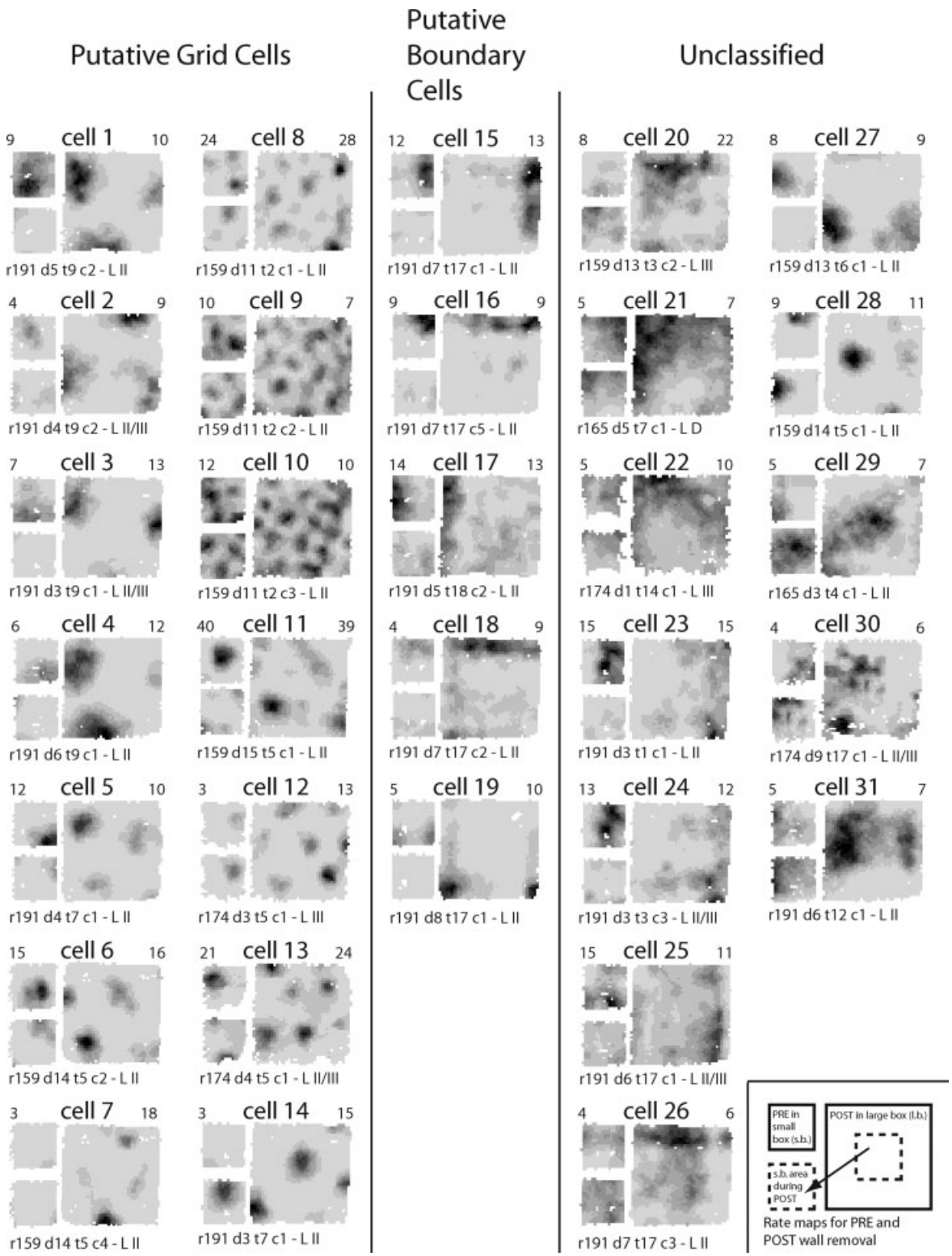

FIGURE 4. Firing rate maps of all putative principal cells (mfr < 10 Hz) with SI > 0.05 bits (see Fig. 3). For each cell, the small map at upper left represents the small box session before the walls were removed (PRE epoch). The large map represents the large-box session after the small-box walls were removed (POST epoch). The small map at the lower left is derived from the large map by including only the pixels covered during the PRE epoch. The same grayscale is shared by all three rate maps of each cell: white denotes unvisited bins, darker shades of gray represent higher firing rates, and black is the highest of the PRE and POST peak rates (top left and right numbers, respectively). Recording information is at the bottom as follows: rat (r), day (d), tetrode (t), unit (c), and MEC layer (L II/III means a precise determination was not possible and L D denotes deep layers). Note that most of the cells shifted their fields in the small-box area after the removal of its delimiting walls.

TABLE 1.

Distance from Dorsal MEC Border, Gridness Scores, and Spatial, Correlation Coefficients for Cells in Figures 4 and 5

Cell ID	Distance from dorsal MEC border (μm)	Gridness score	Small-box area correlation coefficient	Box-rescaling correlation coefficient
Cell 1	1,650	1.15	−0.21	0.00
Cell 2	1,570	0.90	−0.14	−0.31
Cell 3	1,480	0.89	0.03	−0.24
Cell 4	1,730	0.54	−0.17	−0.07
Cell 5	1,150	0.51	−0.29	−0.17
Cell 6	840	0.43	−0.30	0.01
Cell 7	840	0.36	0.35	0.17
Cell 8	310	−0.19	0.08	0.05
Cell 9	310	0.10	0.34	0.13
Cell 10	310	−0.20	0.23	0.00
Cell 11	920	0.04	−0.35	−0.21
Cell 12	380	0.05	0.82	0.00
Cell 13	480	−0.09	−0.28	−0.28
Cell 14	1,070	0.29	−0.29	0.28
Cell 15	910	0.08	−0.06	0.70
Cell 16	910	−0.13	−0.22	0.69
Cell 17	250	−0.15	0.02	0.58
Cell 18	910	−0.07	−0.51	0.46
Cell 19	990	−0.35	0.15	0.72
Cell 20	920	0.18	−0.52	−0.13
Cell 21	2,740	−0.40	0.15	−0.04
Cell 22	2,210	−0.57	0.38	0.22
Cell 23	1,070	−0.28	0.37	0.35
Cell 24	820	−0.06	−0.11	0.04
Cell 25	820	−0.21	0.43	0.29
Cell 26	910	−0.24	0.04	0.08
Cell 27	1,380	0.25	−0.12	0.42
Cell 28	840	0.14	−0.25	−0.17
Cell 29	1,460	−0.21	−0.06	0.26
Cell 30	960	−0.20	−0.27	−0.16
Cell 31	2,390	0.22	0.46	0.29
Cell 32	1,650	−0.02	−0.09	0.66
Cell 33	250	−0.13	0.11	0.64
Cell 34	2,830	−0.15	0.64	0.52

The first column in Figure 4 (Cells 1–7) contains the cells that had a gridness score (Table 1; Sargolini et al., 2006) in the large box that was $\geq$0.3 (which was the cutoff used by Barry et al., 2007). (Only one more cell had a score $\geq$0.3 out of all the remaining spatially informative cells that are not shown in Fig. 4.) The second column (Cells 8–14) contains cells that showed multipeaked firing similar to that of grid cells, but that did not pass the 0.3 gridness score criterion. It is likely that these cells are grid cells whose grid structure was not regular (triangular) enough to pass the stringent grid cell definition of equal-spaced vertices separated by 60° (Hafting et al., 2005), possibly a consequence of the experimental manipulation of the environment boundaries (Barry et al., 2007). For example, cell 12 shows a central vertex surrounded by six peripheral vertices in a hexagonal shape, but the spacing between the vertices is unequal. Cells 8–10 show multipeaked firing patterns that look roughly hexagonal, but with enough distortions to cause the gridness score to drop below the 0.3 criterion.

Inspection of the small-box rate maps of these first two columns (upper left diagram for each cell of Fig. 4) reveals that most of these MEC cells had well-defined place fields that were similar to place fields of the hippocampus proper and that resembled the firing fields reported by Hargreaves et al. (2005) (e.g., Cells 1, 5, 6, 11, and 12). A few cells, recorded dorsocaudally in MEC (Table 1), showed multiple fields in both the small box and large box (Cells 8, 9, and 10). These data are consistent with the idea that the single-peaked place field recordings of the Hargreaves et al. (2005) study were in fact recordings from grid cells, in which only 1 (or 2) grid vertices fit within the confines of the small behavioral chamber. To characterize this result further, we estimated how many cells with single place fields in the small box would be likely to show multiple fields in the large box, based on the recording site along the dorsocaudal-ventrorostral axis of the MEC (Hafting et al., 2005; Sargolini et al., 2006; Brun et al., 2008). We measured the distance from the dorsocaudal border of MEC to the recording site along this axis (Table 1) and extracted the expected intervertex spacing of any grid cell recorded from that location by referring to the data in Supplementary Figure S3 of Sargolini et al. (2006). We estimated that any cell recorded $\leq$1,150 μm from the dorsocaudal MEC border would have an intervertex spacing $\leq$ ~70 cm, approximately half the size of one side of the large box in the current experiment (135 cm × 135 cm). Thus, a conservative estimate was that any cell recorded $\leq$1,150 μm from the dorsocaudal MEC border would have at least two fields in the large box. By visual inspection of Figure 4, Cells 1, 2, 4–7, 11–13, 15–18, 27, and 28 had well-formed, single fields in the small box. As predicted, most of these cells had multiple fields in the large box (even those cells recorded >1,150 μm from the dorsocaudal MEC border).

A distinct class of these cells that did not produce the expected multiple fields in the large box are shown in the third column of Figure 4 ("Putative boundary cells"). These cells tended to fire along a wall or at corners of the small box and big box, with no evidence of a grid-like pattern in either environment. For example, Cells 15–18 fired along one wall in the small box, and they fired along the same wall in the large box, with no evidence of multipeaked firing that would be consistent with a grid cell. Another cell (Cell 19) fired strongly in the same two corners in both the small and large boxes. The firing patterns of these cells scaled with the size of the environment but remained unaltered with respect to its geometry. To quantify this phenomenon, we performed a scaling analysis (Muller and Kubie, 1987; Sharp, 1999; Barry et al., 2007) on all 70 spatially informative cells, in which we correlated the small-box rate map with the large-box rate map scaled down to the same size of the small box area. The five cells described earlier (Cells 15–19) were among the eight cells with the highest correlations. Cells 19, 15, 16 were the highest three (correlation coefficients 0.72, 0.70, 0.69), whereas Cells 17 and 18 were 6th

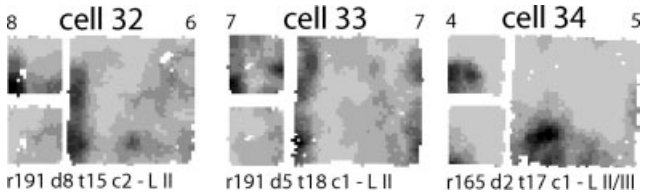

FIGURE 5. Additional examples of putative boundary cells and an ambiguous cell. These cells had spatial information scores in the large box <0.05, so they were not included in Figure 4. However, these cells were among the top 8 in terms of their correlation coefficients between the small box and the rescaled large box. Cells 32 and 33 fired along a wall in both boxes. Cell 34, recorded from a ventral location (Table 1), might have shown a simple grid vertex that either scaled with the environment or just revealed more of the vertex when the small box walls were removed.

and 8th (correlation coefficients 0.58 and 0.46). The remaining three cells are not shown in Figure 4 because they had SI $<$ 0.05 bits. These cells are shown in Figure 5. The two cells that ranked 4th and 5th in terms of the scaled correlations (correlation coefficients 0.66 and 0.64) fired along a wall of the large box and the corresponding wall in the small box (Fig. 5, Cells 32 and 33). The cell ranked 7th (Fig. 5, Cell 34; correlation coefficient 0.52) had one field near the same corner in both the small and large boxes, but the field in the small box could be predicted by either a genuine rescaling of the field in the large box or by the portion of the large-box field occurring in the small box area. Thus, of the cells with the eight highest correlation coefficients in the scaled rate map analysis, at least seven of them fired either at the walls or the corners in both boxes, and none of them fired unambiguously away from the boundaries.

The prevalence of firing of these cells at the walls and corners suggests that they convey information about the boundaries of an environment. Thus, these cells appear to be a different class of cells than the grid cells, even though they were recorded in MEC, less than 1 mm from the dorsocaudal border of MEC (see Fig. 2). The small number of these boundary cells (7 cells) in our sample precludes detailed analysis, but their common origin from three neighboring tetrodes of a single rat suggests that these cells may not be homogeneously distributed in Layer II. Specifically, these cells were recorded from laterally placed tetrodes of this rat ($\sim$5.3–5.7 mm from the midline). Recordings from Layer III with these tetrodes on previous days produced one unit of marginal isolation quality that still showed a grid-like firing pattern, demonstrating that these boundary cells were localized near grid-cell circuits.

The last two columns of Figure 4 ("Unclassified") show the remaining cells with SI $\geq$ 0.05 bits, for which a determination of their specific behavior could not be made either based on the scaling and gridness analyses or according to qualitative visual inspection of their firing rate maps. For example, some of these cells (e.g., Cells 23, 24, and 29) were ambiguous but showed hints of wall-related activity, while others (e.g., Cells 27 and 28) had one or two fields that could in principle be part of a large-scale grid (Brun et al., 2008).

Change of Spatial Response After Boundary Removal

The removal of the small box walls was intended to test whether cells that resembled classic place cells in the small box were revealed to be grid cells in the large box. The earlier analysis showed that many of these cells were grid cells, but others had firing fields that were related to the corners or boundaries of the environment. We were subsequently interested in whether the removal of the small box walls caused changes in the spatial firing locations or firing rates of the cells in general. Because the rat was in the small box when the walls were removed, its path integration system would presumably allow the rat to maintain the firing of the MEC cells in the same location in the large box. Alternatively, the influence of the boundaries of the familiar, large box might cause the firing fields to be altered when the small box walls were removed. To address this question, we first categorized the 31 high-SI cells in Figure 4 by visual inspection of their firing fields. We compared the firing rate maps of the small box (upper left rate map for each cell in Fig. 4) with the firing rate map of the same pixels when the rat was foraging in the large box (lower left rate map for each cell in Fig. 4). Most cells (n = 24) were classified as changing their firing locations (or losing/gaining a firing field) in the small and large box sessions (similar to hippocampal global remapping). For example, Cells 8 and 10 (putative grid cells) shifted the locations of their firing fields; Cells 6, 28, and 30 shifted their single-peaked firing fields; Cells 1 and 15 lost their firing fields within the small-box subregion of the large box; and Cell 14 gained a firing field in this region. The remaining seven cells either did not strongly change their spatial firing pattern in the small-box area (Cell 12) or displayed ambiguous behavior (Cells 3, 7, 9, 22, 25, and 31).

We used three measures to quantify the change of spatial response in the 31 cells shown in Figure 4 as well as in the other 39 spatially modulated principal cells and interneurons. These measures were a rate-change index (defined below) (Fig. 6A); the shift of the COM of the firing rate map (Fig. 6B); and the Pearson correlation between the firing rate maps (Fig. 6C) (Leutgeb et al., 2005). To calculate these values, we first computed smoothed firing rate maps for the small box session before wall removal (PRE); the corresponding area of the large box after wall removal (POST); the first half of the postremoval period (POST1); and the second half of the postremoval period (POST2). The POST epoch excluded the first 2 min to remove any potential response instability or behavioral variability immediately after the wall removal. Only the visited bins, which were confined to the area corresponding to the small box, and which were visited in each epoch were used in the calculation of the mfr and firing rate maps in this analysis.

Figure 6A (top) shows a histogram of the rate change index (|mfr PRE $-$ mfr POST|)/(mfr PRE $+$ mfr POST) between the PRE and POST sessions. The black values are derived from

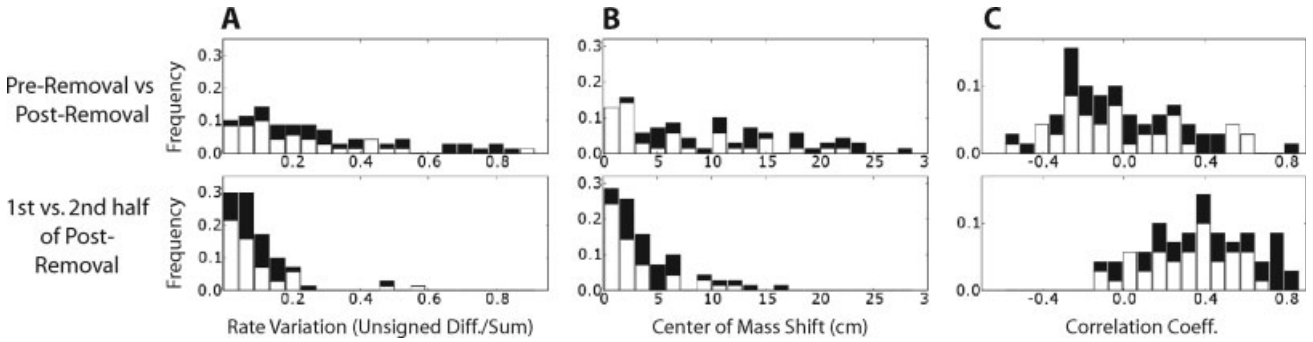

FIGURE 6. Changes in spatial firing patterns and firing rates between the small and large box sessions. All spatially modulated cells were included in the three analyses. Top histograms refer to the change of response between the PRE and POST epochs (before and after the removal of the small box walls). Bottom histograms refer to the change between the first and second half of the POST epoch. In both cases, only the area corresponding to the small box was considered. The black components of histogram bars represent the subpopulation of putative principal cells with high spatial information (SI > 0.05 bits, all the cells displayed in Fig. 4). (A) Population distribution of the rate-change index. (B) Population distribution of the shift of the COM of the firing rate maps. (C) Population distribution of the Pearson correlation between the firing rate maps.

the 31 high-SI cells (Fig. 4), and the white values are derived from the remaining cells. The distribution is highly spread out, with many cells exhibiting marked changes in firing rate between the two sessions. To estimate what the distribution would be with no wall removal, we computed the rate change index between the first and second halves of the POST session (POST1 vs. POST2; Fig. 5B, bottom). The median of the PRE-POST rate change index (0.216) was significantly different than the median of the POST1-POST2 rate change index (0.075; Mann-Whitney test, $P < 0.0001$).

Figure 6B (top) shows a histogram of the change in the COM of the rate maps between the PRE and POST sessions. Many cells showed large changes in the COM (median 7.269 cm). This distribution was significantly larger than the median COM change between the first and second halves of the POST session (median 2.864 cm; Mann-Whitney test, $P < 0.0001$). Finally, Figure 6C (top) shows a histogram of the spatial correlations between the PRE and POST sessions (top) and between the POST1 and POST2 epochs (bottom). The rate maps were significantly less correlated in the PRE–POST comparison than in the POST1–POST2 comparison (medians -0.064 vs. 0.381, Mann-Whitney test, $P < 0.0001$). Thus, for all three measures, greater variability was shown in the responses of the cells between the pre-removal and postremoval periods than between the first and second halves of the postremoval period. These results demonstrate that the removal of the walls caused a significant alteration in the firing patterns of the cells, presumably as the spatial representation was reset/aligned to the new, larger environment.

DISCUSSION

This study describes two main findings. First, comparison of the firing patterns in the small and large boxes revealed that there are at least two classes of spatially modulated neurons in the MEC. One class is composed of the grid cells [and variations of these, such as grid × head direction cells, as shown by Sargolini et al. (2006)]. A second class is composed of cells that fire at the walls or boundaries of the enclosure, regardless of whether it is the small or large box. Cells with a similar behavior have been independently described in preliminary reports (see Moser and Moser, 2008; Solstad et al., 2008). In computational simulations with the oscillatory-interference model of grid-cell dynamics (Burgess et al., 2007), a single reset location along the walls of the environment is sufficient for correcting the progressive drift of the grid representation over time due to noisy self-motion information. Cells firing along boundaries may therefore be useful in binding the grid-cell firing to the boundaries of an environment to keep the internally generated, grid cell representation calibrated with respect to the coordinate frame of the external world. Whether the boundary-related cells of the present experiment fill this hypothesized role requires further, explicit experimental tests.

Second, the results demonstrated strongly that the external boundaries can reset the spatial firing of the MEC cells. Even though the rat was in the small box when the walls were removed, and could presumably continue to path integrate while also perceiving the unaltered global cues to keep the firing fields stable with respect to the absolute coordinate frame of the laboratory environment, most spatial firing fields were altered as a result of the wall removal. Thus, the nearby boundary landmarks overrode the presumptive path integrator, even under conditions when the rat "knew" where it was when the walls were removed.

These results are consistent with previous findings of grid cells and place cells. Initial reports showed that the firing fields of MEC cells were controlled by landmarks, similarly to hippocampal place fields, in that rotation of the landmarks could cause equivalent rotations of the firing fields (Quirk et al., 1992; Hafting et al., 2005). Furthermore, grid cells maintain the same orientation and phase in repeated trials in the same environment, implying that environmental landmarks or boun-

daries must align the internally generated grid with the external world (Hafting et al., 2005). Interestingly, manipulations that cause grid fields to shift relative to environmental boundaries are associated with global remapping of hippocampal place fields, whereas manipulations that do not produce grid shifts are associated with hippocampal rate remapping (Fyhn et al., 2007).

Previous studies of grid cells have altered the size of an environment, although in these studies the manipulation was performed with the rat removed from the enclosure. In one study, grid cells maintained the same spacing between their fields when the environment was scaled, in a situation when both the large and small environments were familiar to the animal (Hafting et al., 2005). However, when the environmental geometry was altered in a novel way in another study, the spacing between grid fields could be stretched or compressed. Barry et al. (2007) recorded grid cells in a square or rectangular chamber with walls that could be moved to change the shape to one of four shapes: a small square, a large square, a vertically oriented rectangle, and a horizontally oriented rectangle. When the environment was stretched from a small square to a vertically oriented rectangle, for example, the spacing between the grid fields stretched asymmetrically, as the spacing grew along the long axis of the rectangle and actually shrunk slightly along the wide axis. As the animal became more familiar with the different geometries, the grid cells maintained the same spacing in all environments (as in Hafting et al., 2005). These experiments demonstrate the strong influence of the environmental boundaries on the firing of grid cells. In this study, we were unable to determine whether the grid scales expanded when the small box walls were removed, because few grid cells in our sample had enough firing fields in the small box to estimate the grid scale. Because both small and big box environments were familiar to the animals after a few days of recording, we would expect that the scales would be minimally affected by this manipulation (Hafting et al., 2005; Barry et al., 2007), although slight distortions in the grid may have resulted from the manipulation (Cells 8–14 of Fig. 4).

Although the environmental landmarks have a strong influence on aligning the MEC firing fields to an allocentric spatial framework, this binding is not absolute. For example, Hargreaves et al. (2007) recorded spatially selective neurons from MEC, parasubiculum, and CA1, as well as head direction cells from the anterior thalamus, in a manipulation where they pitted external landmarks against the rat's idiothetic sense of direction. Rats foraged for food in a square box with a single cue card. In between sessions, the rat was placed in a covered bucket and slowly rotated counterclockwise, presumably below vestibular threshold, while the cue card was rotated clockwise. The rat was then placed back into the square box to determine whether spatial firing fields and head direction tuning curves rotated counterclockwise (indicating control by the idiothetic cues) or clockwise (indicating control by the landmark). In many trials, all spatially tuned firing fields, including those from MEC, were controlled by the idiothetic cues and ignored the salient visual landmark. Thus, like head direction cells and hippocampal place cells (Knierim et al., 1998), idiothetic cues can override the influence of salient landmarks in controlling the firing of MEC cells. In this study, however, the alteration of the environment boundaries had a powerful influence over the idiothetic cues, as most cells changed their firing properties after the wall removal, even though the rat was occupying the space when the manipulation was performed. It is not clear whether the strong influence of the external landmarks in this study was the result of the nature of the landmarks (wall boundaries versus a cue card), the manipulation itself (removing walls in the presence of the rat versus rotating a cue card when the rat was being counter-rotated in a covered bucket), or some other variable (such as amount of experience in the environment). In combination, however, the two studies demonstrate that MEC cells are similar to hippocampal place cells in that the relative influence of self-motion cues versus external landmarks can be a complex interaction dependent on numerous variables.

The boundary-related cells of this study may be relevant to the boundary vector cell (BVC) model of O'Keefe and Burgess (O'Keefe and Burgess, 1996) and Hartley et al. (2000). Similar cells that fire along, or at a distance from, the borders of an environment have been reported in the subiculum (Barry et al., 2006) and parasubiculum (Hargreaves et al., 2005). All of the clear boundary-related cells of this study came from one rat and from three tetrodes localized to the most lateral of the recording locations in the bundle. Moreover, they were all found in or near Layer II. However, in a preliminary report from another lab, Solstad et al. (2008) reported boundary-related cells only in Layers III and V, not Layer II, and found them intermingled with head direction and grid $\times$ head direction cells (see Moser and Moser, 2008). More data will be needed from future studies to characterize the anatomical location of boundary-related cells and whether they display any tendency to distribute nonhomogeneously across different layers and in different regions of the MEC.

In summary, this study sought to determine whether all MEC cells that showed firing fields similar to hippocampal place fields in a small environment were really grid cells that had only one or a few grid vertices in the environment or were a cell type fundamentally different than grid cells. When the walls of the small box were removed, a number of cells were revealed to be grid cells, but other cells appeared to be related to the boundaries or corners of the environment. This latter class fired along the same wall or corners in both small and large box environments, with no grid-like firing patterns. Future experiments will be necessary to test directly the hypothesis that these cells are related to aligning the grid relative to the boundaries of an environment, and to keeping it stable in spite of potential accumulation of self-motion error, as predicted by theoretical work (McNaughton et al., 1996; see also Touretzky and Redish, 1996; Burgess et al., 2007). The powerful influence of the boundaries was demonstrated by the change in spatial firing of almost all cells when the small-box walls were removed in the presence of the rat, revealing the boundaries of the large box. Even though the rat was presumably capa-

ble of maintaining the path-integration-based coordinate frame of the small box as well as of perceiving the unaltered global visual cues, a number of analyses showed that the MEC spatial representation was altered substantially by the manipulation. Because the large box environment was highly familiar to the rat, it remains to be determined whether the same influence would be observed if the rat were familiar only with the small box, and the walls were removed to reveal the large box environment for the first time.

Acknowledgments

The authors thank Geeta Rao for assistance in data collection and Sachin Deshmukh for helpful comments.

REFERENCES

Alonso A, Garcia-Austt E. 1987. Neuronal sources of theta rhythm in the entorhinal cortex of the rat. I. Laminar distribution of theta field potentials. Exp Brain Res 67:493–501.

Barnes CA, McNaughton BL, Mizumori SJ, Leonard BW, Lin LH. 1990. Comparison of spatial and temporal characteristics of neuronal activity in sequential stages of hippocampal processing. Prog Brain Res 83:287–300.

Barry C, Lever C, Hayman R, Hartley T, Burton S, O'Keefe J, Jeffery K, Burgess N. 2006. The boundary vector cell model of place cell firing and spatial memory. Rev Neurosci 17:71–97.

Barry C, Hayman R, Burgess N, Jeffery KJ. 2007. Experience-dependent rescaling of entorhinal grids. Nat Neurosci 10:682–684.

Blair HT, Gupta K, Zhang K. 2008. Conversion of a phase- to a rate-coded position signal by a three-stage model of theta cells, grid cells, and place cells. Hippocampus 18:1239–1255.

Brun VH, Solstad T, Kjelstrup KB, Fyhn M, Witter MP, Moser EI, Moser MB. 2008. Progressive increase in grid scale from dorsal to ventral medial entorhinal cortex. Hippocampus 18:1200–1212.

Burgess N. 2008. Grid cells and theta as oscillatory interference: Theory and predictions. Hippocampus18:1157–1174.

Burgess N, Barry C, O'Keefe J. 2007. An oscillatory interference model of grid cell firing. Hippocampus 17:801–812.

Cover TM, Thomas JA. 2006. Elements of Information Theory. Hoboken, NJ: Wiley-Interscience.

Dolorfo CL, Amaral DG. 1998. Entorhinal cortex of the rat: Topographic organization of the cells of origin of the perforant path projection to the dentate gyrus. J Comp Neurol 398:25–48.

Ego-Stengel V, Wilson MA. 2007. Spatial selectivity and theta phase precession in CA1 interneurons. Hippocampus 17:161–174.

Fox SE, Ranck JB Jr. 1981. Electrophysiological characteristics of hippocampal complex-spike cells and theta cells. Exp Brain Res 41: 399–410.

Frank LM, Brown EN, Wilson MA. 2001. A comparison of the firing properties of putative excitatory and inhibitory neurons from CA1 and the entorhinal cortex. J Neurophysiol 86:2029–2040.

Franzius M, Sprekeler H, Wiskott L. 2007. Slowness and sparseness lead to place, head-direction, and spatial-view cells. PLoS Comput Biol 3:e166. DOI: 10.1371/journal.pcbi.0030166.

Fuhs MC, Touretzky DS. 2006. A spin glass model of path integration in rat medial entorhinal cortex. J Neurosci 26:4266–4276.

Fyhn M, Molden S, Witter MP, Moser EI, Moser MB. 2004. Spatial representation in the entorhinal cortex. Science 305:1258–1264.

Fyhn M, Hafting T, Treves A, Moser MB, Moser EI. 2007. Hippocampal remapping and grid realignment in entorhinal cortex. Nature 446:190–194.

Giocomo LM, Hasselmo ME. 2008. Computation by oscillations: Implications of experimental data for theoretical models of grid cells. Hippocampus 18:1200–1212.

Hafting T, Fyhn M, Molden S, Moser MB, Moser EI. 2005. Microstructure of a spatial map in the entorhinal cortex. Nature 436:801–806.

Hargreaves EL, Rao G, Lee I, Knierim JJ. 2005. Major dissociation between medial and lateral entorhinal input to dorsal hippocampus. Science 308:1792–1794.

Hargreaves EL, Yoganarasimha D, Knierim JJ. 2007. Cohesiveness of spatial and directional representations recorded from neural ensembles in the anterior thalamus, parasubiculum, medial entorhinal cortex, and hippocampus. Hippocampus 17:826–841.

Hartley T, Burgess N, Lever C, Cacucci F, O'Keefe J. 2000. Modeling place fields in terms of the cortical inputs to the hippocampus. Hippocampus 10:369–379.

Hasselmo ME. 2008. Grid cell mechanisms and function: Contributions of entorhinal persistent spiking and phase resetting. Hippocampus 18:1213–1229.

Hasselmo ME, Giocomo LM, Zilli EA. 2007. Grid cell firing may arise from interference of theta frequency membrane potential oscillations in single neurons. Hippocampus 17:1252–1271.

Knierim JJ, Kudrimoti HS, McNaughton BL. 1998. Interactions between idiothetic cues and external landmarks in the control of place cells and head direction cells. J Neurophysiol 80:425–446.

Kropff E, Treves A. 2008. The emergence of grid cells: Intelligent design or just adaptation? Hippocampus 18:1256–1269.

Kubie JL, Muller RU, Bostock E. 1990. Spatial firing properties of hippocampal theta cells. J Neurosci 10:1110–1123.

Leutgeb S, Leutgeb JK, Barnes CA, Moser EI, McNaughton BL, Moser MB. 2005. Independent codes for spatial and episodic memory in hippocampal neuronal ensembles. Science 309:619–623.

Lipton PA, White JA, Eichenbaum H. 2007. Disambiguation of overlapping experiences by neurons in the medial entorhinal cortex. J Neurosci 27:5787–5795.

Marshall L, Henze DA, Hirase H, Leinekugel X, Dragoi G, Buzsaki G. 2002. Hippocampal pyramidal cell-interneuron spike transmission is frequency dependent and responsible for place modulation of interneuron discharge. J Neurosci 22:RC197.

McNaughton BL, Barnes CA, O'Keefe J. 1983. The contributions of position, direction, and velocity to single unit activity in the hippocampus of freely-moving rats. Exp Brain Res 52:41–49.

McNaughton BL, Barnes CA, Gerrard JL, Gothard K, Jung MW, Knierim JJ, Kudrimoti H, Qin Y, Skaggs WE, Suster M, Weaver KL. 1996. Deciphering the hippocampal polyglot: The hippocampus as a path integration system. J Exp Biol 199:173–185.

McNaughton BL, Battaglia FP, Jensen O, Moser EI, Moser MB. 2006. Path integration and the neural basis of the 'cognitive map'. Nat Rev Neurosci 7:663–678.

Miller GA. 1955. Note on the bias of information estimates. In: Quastler H, editor. Information Theory Psychology: Problems Methods Glencoe, Ill.: The Free Press II-B:95–100.

Moser EI, Moser MB. 2008. A metric for space. Hippocampus 18: 1142–1156.

Muller RU, Kubie JL. 1987. The effects of changes in the environment on the spatial firing of hippocampal complex-spike cells. J Neurosci 7:1951–1968.

O'Keefe J, Burgess N. 1996. Geometric determinants of the place fields of hippocampal neurons. Nature 381:425–428.

O'Keefe J, Burgess N. 2005. Dual phase and rate coding in hippocampal place cells: Theoretical significance and relationship to entorhinal grid cells. Hippocampus 15:853–866.

Olypher AV, Lansky P, Muller RU, Fenton AA. 2003. Quantifying location-specific information in the discharge of rat hippocampal place cells. J Neurosci Methods 127:123–135.

Optican LM, Gawne TJ, Richmond BJ, Joseph PJ. 1991. Unbiased measures of transmitted information and channel capacity from multivariate neuronal data. Biol Cybern 65:305–310.

Panzeri S, Senatore R, Montemurro MA, Petersen RS. 2007. Correcting for the sampling bias problem in spike train information measures. J Neurophysiol 98:1064–1072.

Paxinos G, Watson C. 1998. The Rat Brain in Stereotaxic Coordinates, 4th ed. San Diego: Academic Press.

Quirk GJ, Muller RU, Kubie JL, Ranck JB Jr. 1992. The positional firing properties of medial entorhinal neurons: Description and comparison with hippocampal place cells. J Neurosci 12:1945–1963.

Sargolini F, Fyhn M, Hafting T, McNaughton BL, Witter MP, Moser MB, Moser EI. 2006. Conjunctive representation of position, direction, and velocity in entorhinal cortex. Science 312:758–762.

Shannon CE, Weaver W. 1949. The mathematical theory of communication. Urbana: University of Illinois Press.

Sharp PE. 1999. Subicular place cells expand or contract their spatial firing pattern to fit the size of the environment in an open field but not in the presence of barriers: Comparison with hippocampal place cells. Behav Neurosci 113:643–662.

Skaggs WE, McNaughton B, Gothard K, Markus EJ. 1993. An information-theoretic approach to deciphering the hippocampal code. In: Hanson SJ, Cowan JD, Giles CL, editors. Advances in Neural Information Processing Systems, Vol. 4. San Mateo, CA: Morgan Kaufmann. pp 1030–1037.

Skaggs WE, McNaughton BL, Wilson MA, Barnes CA. 1996. Theta phase precession in hippocampal neuronal populations and the compression of temporal sequences. Hippocampus 6:149–172.

Solstad T, Boccara CN, Kropff E, Moser EI, Moser MB. 2008. Border-responsive cells in the medial entorhinal cortex. FENS Abstr 4:128.20.

Touretzky DS, Redish AD. 1996. Theory of rodent navigation based on interacting representations of space. Hippocampus 6:247–270.

Treves A, Panzeri S. 1995. The upward bias in measures of information derived from limited data samples. Neural Comput 7:399–407.

Wilent WB, Nitz DA. 2007. Discrete place fields of hippocampal formation interneurons. J Neurophysiol 97:4152–4161.